Int. J. Bio-Inorg. Hybr. Nanomater., 7(1): 29-42, Spring 2018

Preparation of the novel zeolite AgX/CdO NPs composite catalyst and its application for the effective removal of fenitrothion (FN) from water

S. Yekta[1], M. Sadeghi[2,]*

[1] *Department of Chemistry, Payame Noor University (PNU), Tehran, Iran*

[2] *Department of Chemistry, Lorestan University, Khorramabad, Iran*

Received: 2 October 2017; Accepted: 5 December 2017

ABSTRACT: The novel zeolite AgX/CdO NPs composite catalyst has been fabricated under an ultrasound assisted dispersion route and identified by various analysis including FTIR, XRD, FESEM-EDAX, AFM, TEM, and EDAX-Dot mapping. Afterwards, for the first time, the zeolite AgX/CdO NPs composite has been exerted for the effective removal (adsorption and degradation) of fenitrothion (FN, O,O-dimethyl-O-(3-methyl-4-nitrophenyl phosphorothioate) as an organophosphorus pesticide from water, and the 31PNMR and GC-MS analysis proved its substantial applicability against fenitrothion. The impacts of diverse parameters on the removal outcome of fenitrothion were investigated. The ^{31}PNMR data verified that fenitrothion was removed by the zeolite AgX/CdO NPs composite. To study the reaction kinetic, the first order model was studied. The quantities of the half-life ($t_{1/2}$) and rate constant (k) calculated as 13.91 min and 0.0498 min^{-1}, respectively. The less toxic products of dimethyl phosphorothioic acid (DMPA) and 3-methyl-4-nitrophenol (3-M-4-N) from the degradation and hydrolysis reaction were identified.

Keywords: *AgX/CdO NPs; Composite; Catalyst; Degradation; Fenitrothion; Removal*

INTRODUCTION

The growing population of the world especially in developing countries causes food crisis and this fact makes countries to enhance their agricultural potentials to conquer this imminent crisis. In contrast, the use of different chemical pesticides in many countries is popular as there is no assured infrastructure for farmers to be educated or informed about the modern and healthy procedures in today agriculture than traditional methods. In this regard, the organophosphorus (OP) materials are classified as the largest part of crop protectants (Barr, *et al.*, 2004). The organophosphates are highly toxic artificial compounds which have been using as air fuel constituents, plasticizers, nerve agents in chemical warfare agents, and customarily as pesticides. According to the published reports, five billion pounds of different types of pesticides are annually utilized worldwide. Moreover, 20-38% of the total exerted pesticides include organophosphates. In consequence, this widespread worldwide use of such pesticides especially organophosphate leads to a high risk of water and terrestrial contamination which is also counts as an imminent threat for public health. The exposure to

✉ Corresponding Author - e-mail: meysamsadeghi1177@gmail.com

such chemicals is likely to happen through inhalation of crop dusts, ingestion of contaminated water or food, and the absorption from skin. The toxicity of organophosphates is demonstrated by their role in inhibition of acetylcholinesterase (AChE), an enzyme (Raushel, 2002) that hydrolyses around five thousand acetylcholine (ACh) molecules in each second (Quinn, 1987). Rapid ACh flooding is caused by the AChE inhibition which negatively impacts the body system showing some symptoms such as respiratory disorder, dimmed vision and eye pain, chest pain, and in some drastic cases abdominal pain, vomiting, bladder-bowel malfunction, respiratory deficiency, paralysis and convulsions, and ultimately death. Also, the environmental serious concerns referring to the cholinergic toxicity and, in some other cases, delayed neuropathy are caused by widespread usage of OP materials in agriculture (Casida & Quistad, 2004). In addition to this, the endocrine disruption is linked to some of the thiophosphate pesticides (Tamura, *et al.*, 2001). The other important worldwide issue is how the obsolete pesticides are disposed and treated while the available methods for degradation of these pesticides are not all credible. Fenitrothion (FN, O,O-dimethyl-O-(3-methyl-4-nitrophenyl phosphorothioate) with shown chemical structure in scheme 1, is one of those described OP insecticides. However, fenitrothion is still in use in numerous countries, to protect various agricultural products from vegetable, fruit, to cereals, and more to protect against household insects, and malaria (Meaklim, *et al.*, 2006). Furthermore, fenitrothion is classified as an alternative insecticide for DDT, dieldrin, chlordane, and endrin in the United Nations Environment Program (UNEP) Persistent Organic Pollutants (POPs) (Kanaly, *et al.*, 2005). The olden fenitrothion stocks endanger developing countries, as a UN Food and Agriculture Organization (FAO) report in 1997 unveiled the large values of stored fenitrothion in the Middle East and Africa. These stocks were counted as a serious threat to the environment since they were stored and kept in weak conditions (Kanaly, *et al.*, 2005). Regarding to the above demonstrated issue, an applicable and efficient adsorbent is in need. The zeolites are identified as microporous crystalline aluminosilicate solid structures with specific channels and cavities representing window diameters less than1 nm. This mentioned aluminosilicate framework shows negative charge and can be neutralized by ultra-framework cations. The zeolite framework substantially accommodates various ranges of guest ions and molecules. The zeolites have proved their beneficial potential and applicability in diverse fields and been widely exerted as sorbents, ion exchangers, and catalysts in industrial activities (Sebastian, *et al.*, 2006). Furthermore, the ultra-framework cations (transition metal ions) which are introduced to the zeolites, undeniably grant them efficacious sufficiency and plus enhance their catalytic and adsorption characteristics as these implied cations are commonly unsaturated, represent diverse oxidation states and are able to create various complexes with the guest ions and molecules with higher selectivity than that of filled shell cations (Sebastian, *et al.*, 2006). The synthetic zeolite types of A, X, Y are known as some of the more significant zeolite types which have been widely used in commercial processes (Eskandari, *et al.*, 2017). It is also notable that Milton and Breck declared the discovery of zeolites A and X in 1959 (Eskandari, *et al.*, 2017). As a matter of fact, the zeolite X (NaX or 13X) is defined as a synthetic aluminium-rich analogous of the natural mineral faujasite (Sebastian, *et al.*, 2006). Its framework is formed by the linkage of sodalite cages via double-6-member ring (D6R) which leads to create a large pore diameter of 7.4 Aº (0.74 nm) (Kosanovic, *et al.*, 2011). Also, the high aluminum constituent of zeolite NaX makes it an appropriate adsorbent for the polar molecules (Silva, *et al.*, 2012; Yi, *et al.*, 2012). From the other point of view, the metal oxide nanoparticles have been vastly employed in diverse fields such as ceramic, catalytic, optical, electrical, and others due to their particular physical and chemical properties and also hoisted quantum effects (Somiya & Roy, 2000). TiO_2 (Panayotov & Morris, 2009), Y_2O_3 (Gordon, *et al.*, 2007), ZnO (Becheri, *et al.*, 2008), CaO (Decker, *et al.*, 2002), MgO (Li, *et al.*, 1992), and Fe_3O_4 (Yekta, *et al.*, 2014) can be named as some of the most utilized transition metal oxides which have been synthesized and applied in various scientific works. In fact several methods have been proposed and reported for the synthesis of such noted materials including thermal decomposition (Yang, *et al.*, 2004), sol-gel (Ning, *et al.*, 2004), hydrothermal and solvothermal (Ismail, *et al.*,

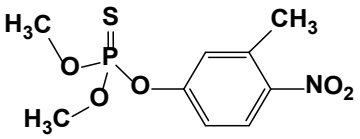

Scheme1. Chemical structure of fenitrothion.

2005), and spray pyrolysis (Saiedi, *et al.*, 2011). The cadmium oxide (CdO) is a known n-type semiconductor with direct and indirect band gaps of 2.2-2.5 eV, and 1.36-1.98 eV respectively (Tadjarodi, *et al.*, 2013; Akin, *et al.*, 2013; Kaviyarasu, *et al.*, 2014). The observed variation in both direct and indirect band gaps is corresponded to the indigenous cadmium and oxygen vacancies. The characteristics like having ionic nature along with low electrical resistance and also enhanced optical transmission in the visible zone, nominate the CdO nanoparticles (CdO NPs) as appropriate alternative for different applications including photovoltaic cells (Jadduaa, *et al.*, 2016), IR reflectors (Tripathi, *et al.*, 2016), transparent electrodes (Wu, *et al.*, 1997), optical coatings (Ghosh, *et al.*, 2007), phototransistors (Su, *et al.*, 1984), and also gas sensors (Krishnakumar, *et al.*, 1984). Further, several synthesis processes have been proposed to prepare the CdO NPs such as solvothermal (Ghosh & Rao, 2004), thermal decomposition (Yufanyi, *et al.*, 2014), hydrothermal (Yang, *et al.*, 2010), sonochemical (Askarinejad & Morsali, 2008), and mechanochemical (Tadjarodi & Imani, 2011) methods. In this investigation, for the first time, the novel zeolite AgX/CdO NPs composite catalyst was synthesized by the ultrasound assisted dispersion method and successfully utilized for the effective removal (adsorption and degradation) of organophosphorus fenitrothion (FN) insecticide from aqueous solution.

MATERIAL AND METHODS

Materials

Sodium silicate (Na_2SiO_3), aluminum hydroxide ($Al(OH)_3$), silver nitrate ($AgNO_3$), cadmium nitrate hexahydrate ($Cd(NO_3)_2.6H_2O$), and sodium hydroxide (NaOH) were all utilized as precursors for the synthesis of the catalysts. Besides, fenitrothion (FN, O,O-dimethyl-O-(3-methyl-4-nitrophenyl phosphorothioate), n-octane, phosphoric acid (H_3PO_4), chloroform-d ($CDCl_3$) and dichloromethane (CH_2Cl_2) were employed for the understudy removal reactions. All of the necessary chemicals were purchased from Merck (Germany) and Sigma-Aldrich (USA), and used as received. Also, the deionized water was exerted throughout the work.

Instrumentation

To prepare the composite, an ultrasonic apparatus was operated at 37 kHz (Sonic 6MX; output acoustic power=100W). The FTIR study was accomplished by a Schimadzu system FTIR 160 spectrophotometer in the wavelength range of 400-4000 cm^{-1} with KBr pellets and the subsequent spectra were recorded and meticulously analyzed. Moreover, the powder X-ray diffraction (XRD) patterns were obtained via a Philips X'pert Pro diffractometer with CoKα radiation at wavelength of 1.54056 Å (30 mA and 40 kV) at room temperature. Its resulted data were provided in the range of 4-80° in 2θ with a scanning speed of 2° min-1. Further, a field emission scanning electron microscopy□energy□dispersiveX□rayspectroscopy(FESEM□EDAX) and X-ray Mapping on a MIRA3 TESCAN scanning electron microscope eqquiped with an energy□dispersive X□ray was operated to investigate the elemental analysis and morphology of the prepared catalyst samples. The atomic force microscope (AFM) of Danish Micro Engineering (DME)/(A/S DK-2730) was exerted for the prepared samples and the related investigations were carried out in non-contact condition at room temperature. The size of the synthesized particles was evaluated using a transmission electron microscopy (TEM) on an EM10C microscope working at an increasing voltage of 100 kV. The characterization studies continued engaging a Bruker DPX-250 spectrometer producing 250 MHz Radio Frequency (RF) by which the Phosphorous-31 Nuclear Magnetic Resonance (^{31}PNMR) spectra were gained and recorded. A VARIAN SATURN4D GC coupled to a DB 5 mass spectrometer and 0.1 micron capillary column (30m length, 0.25 mm i.d.) was operated to provide the gas chromatography-mass spectrometry (GC-MS) analysis for the treated samples. The injector temperature of 250ºC, column temperature setting of 50ºC (6min) at 8ºC/min-100ºC (12 min) at 20ºC/min-250ºC

(6 min), helium as carrier gas (99.999% purity) at flow rate of 10 mL/min, were selected as the GC operating conditions for the products. Besides, a Universal, CAT. NO. 1004 centrifuge instrument was operated throughout the experiments.

Synthesis of zeolite NaX by the hydrothermal method

In this way, primarily 4.2 g of aluminum hydroxide ($Al(OH)_3$) was precisely measured and added to 8.4 mL of sodium hydroxide (NaOH) aqueous solution (50 % w/v) at 100°C. Afterwards, 8.5 mL of deionized water poured into the solution. Then, 15.1 g of sodium hydroxide dissolved into the supplied mixture and another 60 mL of the deionized water was poured and pursuantly heated to meet 50°C (solution A). To prepare the solution B, 45.2 g of sodium silicate (Na_2SiO_3) was introduced-dissolved into a mixture which contained 15.2 g of sodium hydroxide in 250 mL of deionized water. These supplied solutions (A and B) were mixed vigorously and the resulted solution was then heated at 70°C in oven and the obtained white powder (product) was washed by the deionized water and plus dried at 80°C (Abdi, *et al.*, 2014).

Preparation of zeolite AgX by the ion exchange method

For this goal, 5 g of the zeolite NaX which was previously synthesized placed in the furnace at 400°C for 2h to be perfectly calcined. This calcined zeolite NaX was introduced to a 50 mL of a 0.15 M silver nitrate ($AgNO_3$) solution and the prepared mixture was then undergone magnetic stirring at 50°C for 4h to perform the ion exchange phenomenon by which the Ag+ ions occupied the positions of Na^+ ions in the zeolite structure. Afterwards, to remove the excessive salt ions, the obtained zeolite was suitably filtered and washed by the deionized water and subsequently dried at 110°C for 16h. Consequently, the resultant dried zeolite AgX was calcined at 400°C for 3h.

Preparation of zeolite AgX/CdO NPs composite by the ultrasound assisted dispersion method

In order to prepare this composite, initially, 1.5 g of cadmium nitrate hexahydrate ($Cd(NO_3)_2.6H_2O$) was dissolved to the 250 mL of deionized water and further included in an ultrasonic irradiation under for 40 min. Next, 4.5 g of the pre-synthesized zeolite AgX was added to the prepared suspension of the nanoparticles and the provided mixture was intensively shaked for ongoing 12h. In fact, the shaking helps the CdO NPs to be deposited on the surface of the zeolite AgX. Moreover, the gained mixture was filtered and then dried at 110°C for 24h and the ultimate sample was calcined in the furnace at 550°C for 5h.

Removal tests

The removal reactions of the fenitrothion insecticide from aqueous solution were surveyed in the presence of zeolite AgX/CdO NPs composite under ^{31}PNMR and GC-MS analyses. Four main stages were designed and implemented for the preparation of samples. In this matter, at first stage, a 25 mL of 0.03 M phosphoric acid (H_3PO_4) solution was prepared and considered as the blank solution and then injected to a capillary column with heated closed tips (solution A). At second stage, to prepare the solution B, the quantities of 50, 100, 150, 200 and 300 mg/L of fenitrothion was added to 3 mL of a 2:1 (v/v) ratio of water: n-octane as the solvent. The third stage comprises the addition of different amounts of 0.02, 0.04, 0.06, 0.08, 0.1 and 0.2 g zeolite AgX/CdO NPs composite catalyst to the solution B prepared solutions separately and then mixing them in six 50 mL Erlenmeyer flasks with vigorous stirring for 5, 10, 15, 20, 25 and 30 min (solution C). At the fourth stage, the volume of 1 mL of every supplied solutions C was poured into centrifuge tubes and the device operated at 600 rpm for 6 min. Besides, 0.3 mL of the previously implied samples and also 0.2 mL of chloroform-d ($CDCl_3$) were poured into NMR tubes along with the capillary column (solution A). In consequent, the ^{31}PNMR investigation was employed to indicate the values of fenitrothion in the understudy samples. Also, to provide more sufficient quantitative viewpoint, the volume of 10 µL of each upper solution was brought out by a micro-syringe and injected to the GC-MS device.

RESULTS AND DISCUSSION

FTIR

The FTIR analysis was performed for all of the pre-

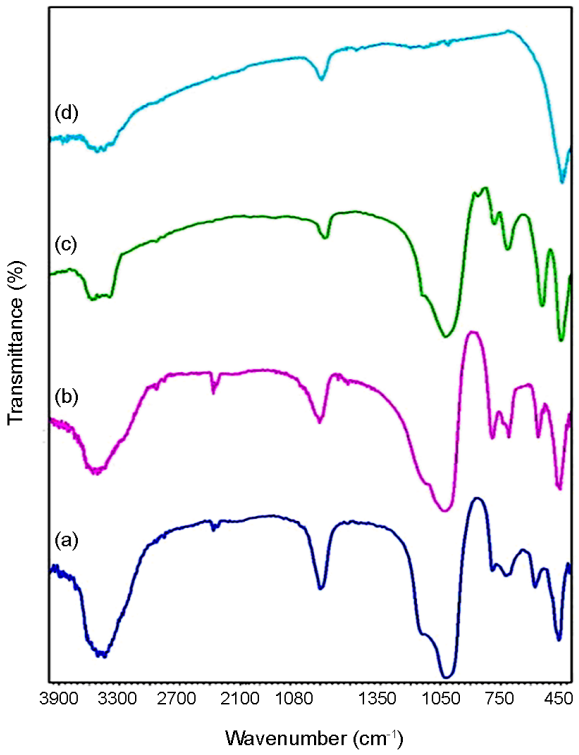

Fig. 1. FTIR spectra of: a) initial NaX, b) AgX, c) AgX/CdO NPs, and d) raw CdO NPs.

pared samples. Therefore, the affiliated spectra of the initial zeolite NaX (Fig. 1a), zeolite AgX (Fig. 1b), zeolite AgX/CdO NPs composite (Fig. 1c) and raw CdO NPs (Fig. 1d), have been respectively represented in Fig. 1. According to the recorded spectra, it is deduced that the appeared peaks positions are nearly equivalent for those three zeolites X included samples. The hydroxyl groups (H-O-H bending and O-H bonding) vibrations and plus segregated H_2O absorption bands in the zeolite X, lead to form peaks around 3560 cm^{-1} and 1652 cm^{-1} respectively. Furthermore, the emerged peaks at 972 cm^{-1} can be attributed to the external connection and also internal tetrahedral asymmetrical stretching vibrations. The internal tetrahedral symmetrical stretching vibrations and external connection make the peaks appear at about 750 cm^{-1} and 669 cm^{-1} respectively. Moreover, the double six rings (D6R) external linkage and plus bending vibrations of the insusceptible internal SiO_4 or AlO_4 tetrahedral units in the zeolite X structure cause the happened peaks about 561 cm^{-1} and 457 cm^{-1} respectively. Based on the observed results gathered from Figs. 1b and 1c, the immobilization and ion exchange processes had caused no tangible change or deformation in the zeolite framework as there has been no citable variation in the bands of zeolite AgX and also zeolite AgX/CdO NPs composite in comparison with those of zeolite NaX. Elsewhere, a bond of Cd-O-Si and/or Cd-O-Al which is attributed to the immobilized CdO NPs in the structure of zeolite causes a new peak at 868 cm^{-1} as can be seen in Fig. 1c. Meanwhile, from the FTIR spectrum of raw CdO NPs in Fig. 1d, the broad identified absorption peaks at around 3570 cm^{-1} and 1631 cm^{-1} are assigned to the adsorbed H_2O molecules. In addition, the stretching vibrations of Cd-O bonding created a peak at 450 cm^{-1}.

XRD

The structural features of the prepared samples were investigated and determined by Powder X-ray diffraction patterns. The related XRD patterns of the initial zeolite NaX (Fig. 2a), zeolite AgX (Fig. 2b), zeolite AgX/CdO NPs composite (Fig. 2c) and raw CdO NPs (Fig. 2d), have been respectively illustrated in Fig. 2. From these patterns, a series of sharp peaks corresponded to the three type zeolite X emerged at 2θ values of 7.1508° to 35.3467° were created by the diffraction planes of (111) to (503), respectively. They were in good consistency with the defined values for the zeolite NaX with JCPDS card NO. 041-0118. The ion exchange and immobilization procedures which were implemented in order to introduce the Ag^+ and CdO NPs to the framework of zeolite NaX to create zeolite AgX/CdO NPs composite caused no destructive effect on the zeolite structure. The immobilization of the synthesized CdO NPs as the guest materials on the zeolite AgX considered as the host material caused five more clear peaks which were observed at 2θ of 33.001°, 38.285°, 55.258°, 65.91°, and 69.288° relating to the diffraction planes of (111), (200), (220), (311), and (222), respectively. Besides, during the immobilization process of CdO species, no characteristic peak referring to the impurities presence was identified in the provided patterns. Further, by using the Debye-Scherrer eq. (1) the crystalline size of the synthesized CdO NPs immobilized on the zeolite AgX was measured:

$$D_{XRD} = \frac{0.9\lambda}{\beta \cos\theta} \quad (1)$$

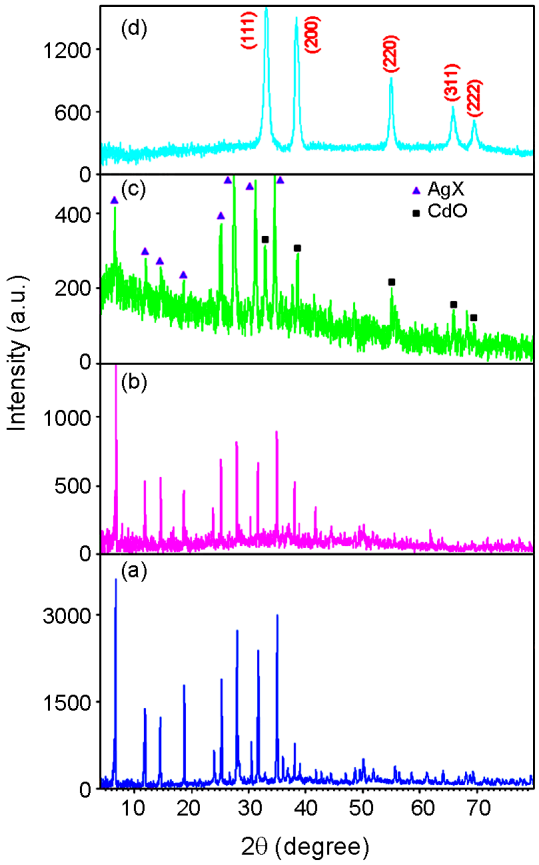

Fig. 2. XRD patterns of: a) initial NaX, b) AgX, c) AgX/CdO NPs, and d) raw CdO NPs.

In the represented equation, the average crystallite size is specified as DXRD, the wavelength of CoKα radiation is shown as λ, the full width at half maximum (FWHM) of the considered diffraction peak is defined as β and θ is referred to the Bragg diffraction angle. Meanwhile, some peaks assigned to the raw CdO NPs appeared at scattering angles of 2θ= 33.073°, 38.298°, 55.264°, 65.94°, and 69.289° relating to the diffraction planes of (111), (200), (220), (311), and (222), respectively which were in great consistency with those of CdO NPs (FCC phase, JCPDS card NO. 75-293). From the above mentioned equation, the average particle size for CdO NPs in the zeolite AgX/CdO NPs composite is calculated 12.5 nm.

FESEM

The crystalline size and morphology of the initial zeolite NaX (Fig. 3a), zeolite AgX (Fig. 3b), zeolite AgX/CdO NPs composite (Fig. 3c) and raw CdO NPs (Fig. 3d) were all determined via FESEM technique as have been respectively depicted in Fig. 3. The expected homogeneous morphology of the zeolite NaX and further quasi-spherical shape of the CdO NPs significantly immobilized on the initial zeolite AgX can be comprehensively described by FESEM micrographs. Looking crossly to the obtained images, again it is emphasized that there is no sign of deformation or destructive impact related to the ion exchange/immobilization stages on the crystallinity and morphology of the zeolite NaX or zeolite AgX/CdO NPs composite frameworks. The estimations revealed the average crystalline size of less than 30 nm (nanometric range) for the CdO NPs in the fabricated composite.

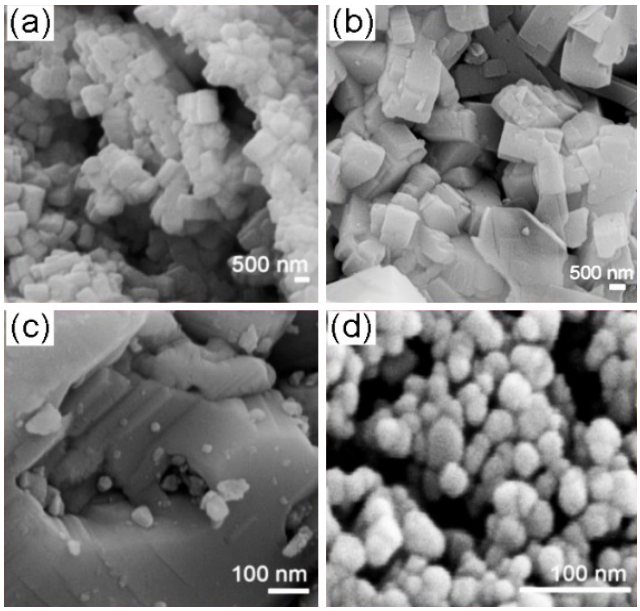

Fig. 3. FESEM micrographs of: a) initial NaX, b) AgX, c) AgX/CdO NPs, and d) raw CdO NPs.

AFM and TEM

The atomic force microscopy (AFM) micrograph affiliated to the zeolite AgX/CdO NPs has been illustrated in Fig. 4a. The investigation of the interaction forces corresponded to the tip and the sample surface

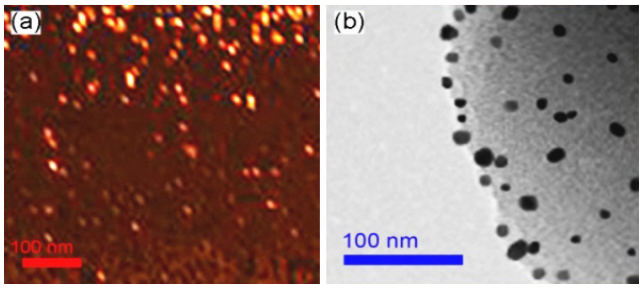

Fig. 4. AFM micrograph of: a) AgX/CdO NPs, and TEM micrograph of: b) AgX/CdO NPs.

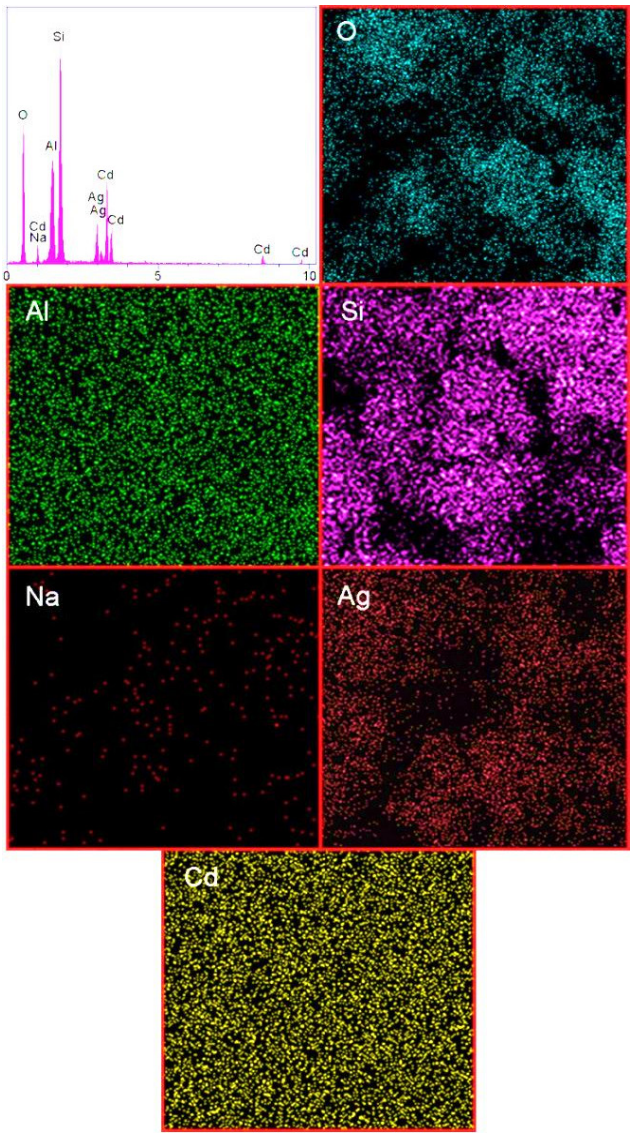

Fig. 5. EDAX analysis of: AgX/CdO NPs, and d) EDAX dot-mappings of the AgX/CdO NPs that indicates the locations of different element across the composite framework.

attained the AFM micrograph. However, according to the AFM micrograph, the mediocre particle size was estimated to be less than 20 nm for the CdO NPs in the AgX/CdO NPs. Also, Fig. 4b contains the corresponding TEM micrographs of the zeolite AgX/CdO NPs composite. According to these micrographs, the average particle size of 12 nm for CdO NPs was indicated and meanwhile the narrow particle size distribution of these particles in the synthesized zeolite AgX/CdO NPs composite was verified. It is also noteworthy that the gathered data from the TEM micrographs were similar to the average particle size which was indicated throughout the XRD, FESEM and AFM analysis.

EDAX

To provide a better view of the elemental composition of the synthesized zeolite AgX/CdO NPs composite, the energy dispersive X-rays (EDAX) analysis was also applied as the resulted outcome has been demonstrated in Fig. 5. From the spectra, the presence of O, Al, and Si elements in the zeolite AgX/CdO NPs composite structure is strongly acknowledged which corroborates the collected results from the XRD patterns. Also, the seven identified peaks for each of Ag and Cd in Fig. 5 spectrum, clearly proves the presence of these elements in the AgX/CdO NPs composite structure. In this regard and according to the provided data, the coexistence of 6.4wt.% Ag and 17.8wt.% CdO in the composite framework is explicitly corroborated. Additionally, the SEM micrographs of the synthesized composite along with the related EDAX elemental dot-mappings have been depicted in Fig. 5. In the elemental map, a higher concentration of the corresponding element has been characterized as a brighter area. To provide a better understanding about these elements positions within the nanomaterials, each element was denoted with a specific color. From the elemental mappings distributions (Fig. 5), the presence of O, Al, Si, Na, Ag, and Cd can be vividly verified. Moreover, considering the maps, the homogeneity of the sample which is defined as the uniform distribution of elements over the composite is definitely acknowledged.

Removal of fenitrothion using the AgX/CdO NPs

Effect of contact time

To figure out the optimum time interval for the high yield removal (adsorption-degradation) reaction of fenitrothion insecticide over the zeolite AgX/CdO NPs composite catalyst, diverse time ranges were separately considered through different consecutive experiments. These series of experiments clarified the direct dependency between reaction time and the efficiency of removal reaction. In this matter, the variation between removal efficiency (%) of fenitrothion against contact time on the synthesized zeolite AgX/CdO NPs composite catalyst has been described in Figs. 6 and 7. Thereupon, a range of 0-30 min was examined for the removal process and the collected data showed the highest removal efficiency for the

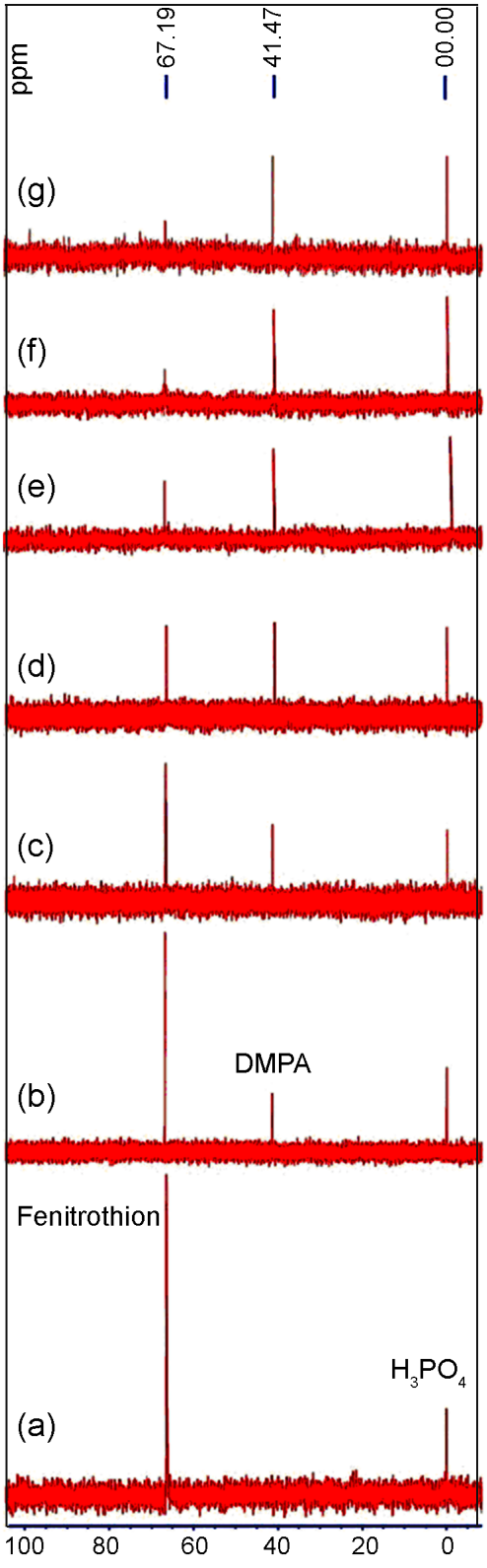

Fig. 6. ^{31}PNMR spectra of fenitrothion-AgX/CdO NPs sample; the following structural assignments were made at δ= 67 ppm (fenitrothion), δ= 41 ppm (DMPA) and δ= 0 ppm (H_3PO_4), at various contact times, a) 0, b) 5, c) 10, d) 15, d) 20, e) 25, and e) 30 min (catalyst dose= 0.06 g/L, initial concentration= 50 mg/L).

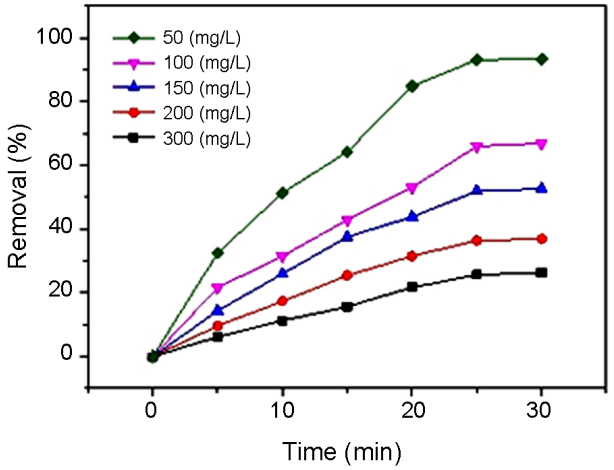

Fig. 7. Effect of contact time on the removal of fenitrothion using the AgX/CdO NPs at different initial concentrations.

contact time of 5min. Also, to study the progress of the removal reaction and on the other hand to emphasize the particular potential of the zeolite AgX/CdO NPs composite catalyst in the adsorption-degradation of fenitrothion, the ^{31}PNMR was also operated. Phosphoric acid (H_3PO_4) as the internal standard, the temperature of 25°C and 25 min as the optimum shaking time were selected as operating parameters for the ^{31}PNMR, respectively.

The ^{31}PNMR results indicate three narrow chemical shifts (δ). Two chemical shifts around δ=67 and δ=0 ppm are caused by fenitrothion and H_3PO_4 respectively. A chemical shift around δ=41 ppm is attributed to the dimethyl phosphorothioic acid (DMPA). The degradation value was indicated by measuring the integrated AUC data of two samples of fenitrothion and H_3PO_4 for all variables and the ratio of integrated AUC of fenitrothion to integrated AUC of H_3PO_4 was also determined. Further, the area under curve (AUC) integral information under above specified factors of ^{31}PNMR can be observed in Figs. 6 and 7, and Table 1.

Effect of catalyst dose

In the current study, to identify the optimized quantity of the catalyst and fulfill the high yield removal process, a range of 0.02-0.2 g of zeolite AgX/CdO NPs composite catalyst was selected for the removal of fenitrothion. Based on the observations from Fig. 8, the higher the catalyst dose the more the removal efficiency until the point that no more change is happened

Table1. ^{31}PNMR spectra results for fenitrothion-AgX/CdO NPs samples under optimum conditions: initial concentration= 50 mg/L, catalyst dose= 0.06 g/L.

Time (min)		Fenitrothion (δ= 67 ppm) AUC Intg	H_3PO_4 (δ= 0 ppm) AUC Intg	Fenitrothion (AUC Intg /H_3PO_4 AUC Intg)
a	0	6.0346	1.0000	6.0346
b	5	4.6843	1.0000	4.6843
c	10	2.9340	1.0000	2.9340
d	15	2.1567	1.0000	2.1567
e	20	0.9136	1.0000	0.9136
f	25	0.4133	1.0000	0.4133
g	30	0.4043	1.0000	0.4043

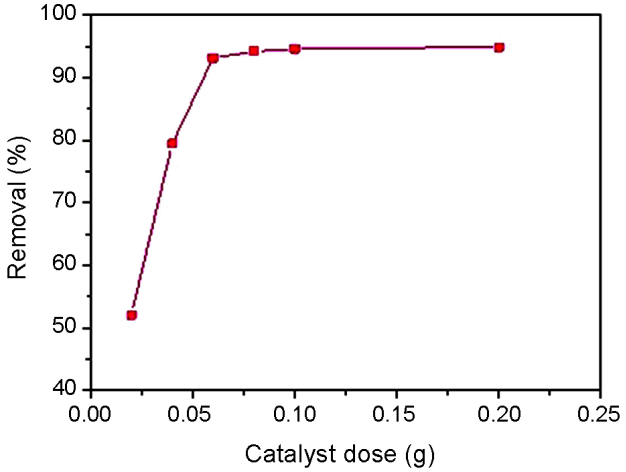

Fig. 8. Effect of catalyst dose on the removal of fenitrothion using the AgX/CdO NPs (optimum conditions: initial concentration: 50 mg/L, and contact time: 25 min).

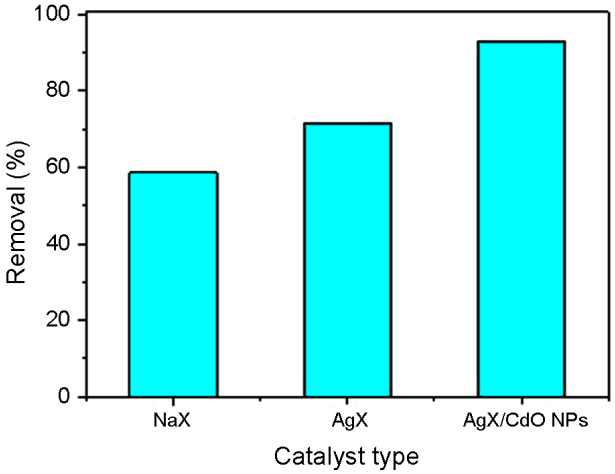

Fig. 9. Effect of catalyst type on the removal of fenitrothion using the AgX/CdO NPs (initial concentration: 50 mg/L, and contact time: 25 min).

and the curve slope goes to linear form which shows a constant value. In consequence, 0.06 g of zeolite AgX/CdO NPs composite catalyst was selected as the optimized value to be used in ulterior experiments.

Effect of catalyst type

In order to evaluate the function of each zeolite NaX, zeolite AgX and zeolite AgX/CdO NPs composite catalyst against fenitrothion and to provide a reliable comparison among these three prepared adsorbents applicability for removal, they were examined in three separate experiments. All of those three catalysts were employed in the same experimental conditions for the above-noted series of experiments. According to Fig. 9, the highest removal (adsorption and degradation) is attributed to the zeolite AgX/CdO NPs composite as its removal efficiency is considerably higher than those two other adsorbents.

Kinetics determination

The removal kinetics was studied using the plots of Ln (fenitrothion concentration) against reaction time and the relevant results were shown in Fig. 10. Meanwhile, the removal rate constant (slope), k, was calculated from the first order equation: Ln C_o/C_t= kt.

In the introduced equation, C_o is defined as the initial concentration, C_t is attributed to concentration of the fenitrothion at time t, and k is the rate constant of removal. Elsewhere, using the equation of $t_{1/2}$= Ln/k, the $t_{1/2}$ (half-life) quantity is sufficiently measured. Thus, the experiments regarding to the adsorption kinetics were carried out as 0.06 g of zeolite AgX/CdO NPs composite catalyst was added into the separate containers each having 50 mg/L of fenitrothion at certain time intervals. The related data have been registered in Table 2.

Table2. First order kinetic parameters for the removal of fenitrothion using the AgX/CdO NPs at different initial concentrations (optimum conditions; contact time: 25 min and catalyst dose: 0.06 g).

Initial concentration (mg/L)	Half-life ($t_{1/2}$, min)	Rate constant (k, min^{-1})	First order kinetic equation
50	13.91	0.0498	$Ln\ C_o/C_t = 0.0498t-0.1549$
100	36.47	0.019	$Ln\ C_o/C_t = 0.019t+0.0164$
150	52.90	0.0131	$Ln\ C_o/C_t = 0.0131t+0.0334$
200	78.75	0.0088	$Ln\ C_o/C_t = 0.0081t+0.0252$
300	130.75	0.0061	$Ln\ C_o/C_t = 0.0053t+0.0131$

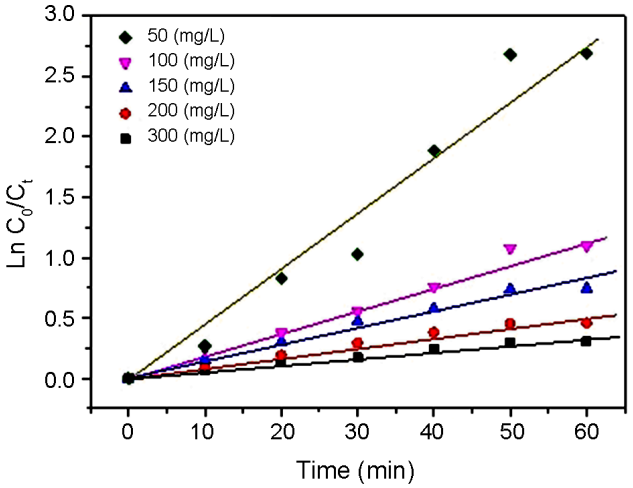

Fig. 10. Linear plots of Ln C_o/C_t against contact time on the removal of fenitrothion using the AgX/CdO NPs at different initial concentrations.

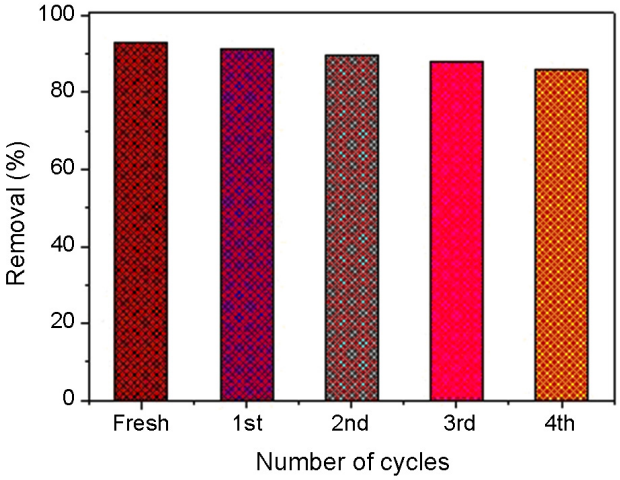

Fig. 11. Recyclability of the zeolite AgX/CdO NPs composite catalyst (initial concentration: 50 mg/L, and contact time: 25 min, and catalyst dose= 0.06 g/L).

Recyclability of the AgX/CdO NPs

To evaluate the applicability of the used catalyst for multiple times of functioning, the spent zeolite AgX/CdO NPs composite catalyst was immersed in the dichloromethane (CH_2Cl_2) solution along with stirring for 1h at certain temperature. When the washing step by the above cited mixture is fully accomplished, the fenitrothion is expected to be desorbed from the composite catalyst. Then, this regenerated catalyst was dried and applied for extra removal experiments. After the first cycle, a trivial decrease was specified in the regeneration efficiency of the zeolite AgX/CdO NPs composite. Nevertheless, the synthesized catalyst attained high removal efficiency for some ulterior cycles. As it has been demonstrated in Fig. 11, the catalyst was recovered four times and the removal efficiency was measured more than 85.9% for those cycles.

GC-MS

The degradation and hydrolysis products of fenitrothion on the zeolite AgX/CdO NPs composite catalyst were identified using a gas chromatography-mass spectrometry (GC-MS). The mass spectra of fenitrothion, 3-methyl-4-nitrophenol (3-M-4-N) mi and dimethyl phosphorothioic acid (DMPA) with retention times of 16.1, 14.7 and 12.6 min respectively have been demonstrated in Fig. 12 which attains an explicit view of the degraded fenitrothion and emerging removal products. Also, the GCMS detector was set to scan a mass scope of 111, 95, 79, 63, 47, and 32 m/z, 153, 125, 109, 75, and 32 m/z, and 277, 263, 247, 214, 150, 125, 93, 79, and 63 m/z for DMPA, 3-M-4-N and fenitrothion, respectively.

Mechanism discussion

As can be seen in scheme 2, two main steps are pro-

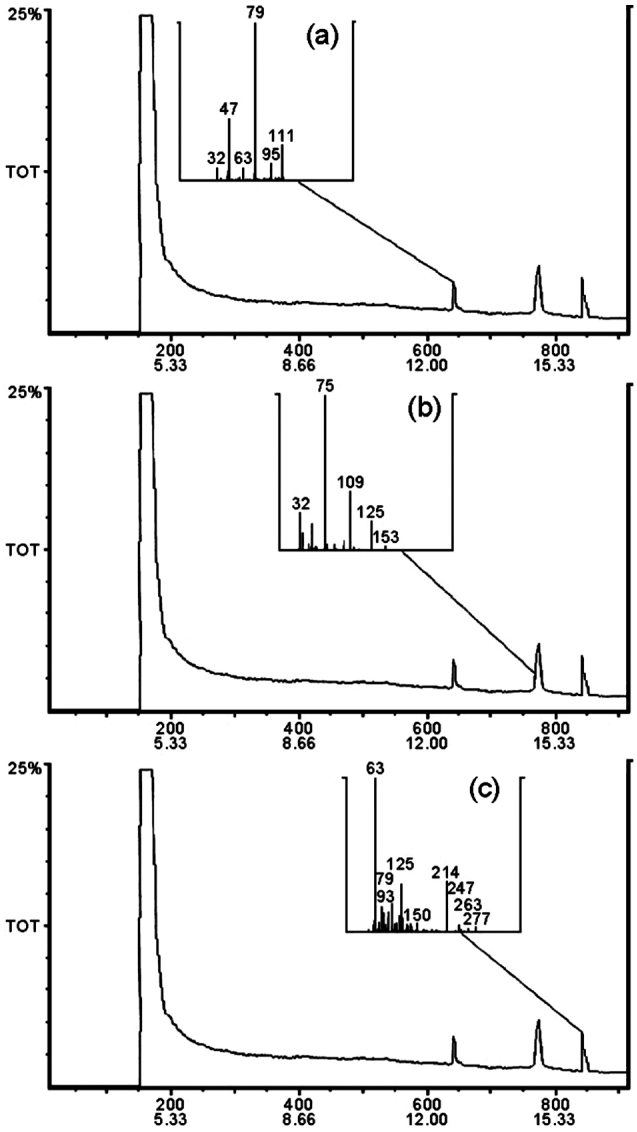

Fig. 12. GC-MS analysis of the degradation and hydrolysis products of the AgX/CdO NPs reaction with fenitrothion: a) DMPA, b) 3-M-4-N, and c) fenitrothion.

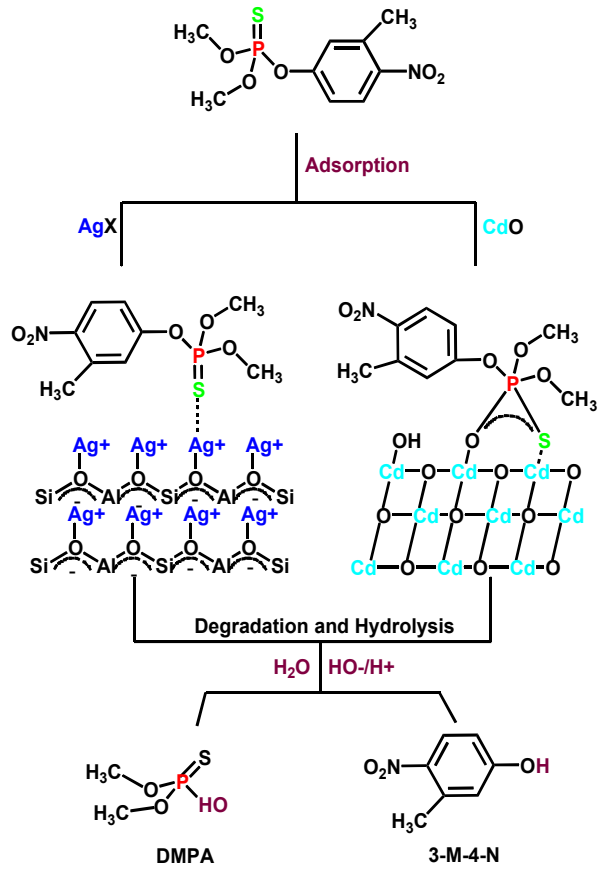

Scheme 2. Reaction mechanism pathway for the removal of fenitrothion using the zeolite AgX/CdO NPs composite.

posed for the removal mechanism. Step (1) the metal ions from zeolite AgX and CdO NPs including Ag^{+} and Cd^{2+} act as Lewis acid sites and link to the sulfur atom in P=S bond referring to their electrophilic behavior. This described linkage of those metal ions with sulfur atoms enhance the electrophilic inclination of the phosphorus and makes it very vulnerable against probable H_2O (H^{+}/OH^{-}) attacks in sequential steps. At step (2), after the adsorption of fenitrothion over the zeolite AgX/CdO NPs composite catalyst, the P-O bonds of the P-O-C_{Aro} break in presence of water molecules behaving as nucleophiles. Moreover, two metal atoms build the surface bound of Cd-O-P-S-Cd and the fenitrothion remains on the surface of the catalyst by phosphoryl sulfur and phosphoryl oxygen bonds. In consequence, the 3-methyl-4-nitrophenol (3-M-4-N) and dimethyl phosphorothioic acid (DMPA) as two less toxic removal products of fenitrothion left the catalyst and entered into the solution.

CONCLUSIONS

The current research focuses on the synthesis and application of the zeolite AgX/CdO NPs composite catalyst for the removal (adsorption-degradation) of fenitrothion (O,O-diethyl-S-(2-ethylthioethyl) thiophosphate) from aqueous solution. The ultrasound assisted dispersion route was applied for the synthesis of zeolite AgX/CdO NPs composite catalyst. Besides, the morphological, structural and crystalline size of the zeolite AgX/CdO NPs composite catalyst were all investigated by various characterization techniques. Also, ^{31}PNMR analysis confirmed the successful removal of the specified organophosphorus material

from the aqueous media. Contact time, initial concentration, catalyst dose and catalyst type as some substantial parameters on the removal efficiency of fenitrothion were precisely studied and the optimized values indicated. The ^{31}PNMR results described that the fenitrothion was comprehensively degraded by the synthesized composite catalyst with a yield of 93.15% under optimized experimental conditions. Meantime, using the first order model, the reaction kinetic data was specified and the affiliated quantity of the half-life (t1/2) and rate constant (k) have been calculated to be 13.91 min and 0.0498 min-1, respectively. In addition, the characterizations collected results all corroborated the significant potential and reliable functionality of the composite catalyst for the removal of fenitrothion. Ultimately, the 3-methyl-4-nitrophenol (3-M-4-N) and dimethyl phosphorothioic acid (DMPA) as the less-toxic degradation products of fenitrothion on the zeolite AgX/CdO NPs composite catalyst were acquired.

ACKNOWLEDGMENT

The authors give their sincere thanks to the Payame Noor University, Ramsar, Iran for all sincere supports.

REFERENCES

Abdi, M.R.; Shakur, H.R.; Rezaee Ebrahim Saraee, K.h.; Sadeghi, M.; (2014). Effective removal of uranium ions from drinking water using CuO/X zeolite based nanocomposites: effects of nano concentration and cation exchange. J. Radioanal. Nucl. Chem., 300(3): 1217-1225.

Akin, S.; Karanfil, G.; Gültekin, A.;.Sonmezoglu, S.; (2013). Improvement of physical properties of CdO thin films by Au–Ag nanocluster codoping, J. Alloys. Compd., 579(1): 272-278.

Askarinejad, A.; Morsali, A.; (2008). Syntheses and characterization of CdCO3 and CdO nanoparticles by using a sonochemical method. Mater. Lett., 62(3): 478-482.

Barr, D.B.; Bravo, R.; Weerasekera, G.; altabiano, C L.M.; Whitehead, R.D.Jr.; Olsson, A.O.; Caudill, S.P.; Schober, S.E.; Pirkle, J.L.; Sampson, E.J.; Jackson, R.J.; Needham, L.L.; (2004). Concentrations of dialkyl phosphate metabolites of organophosphorus pesticides in the U.S. population. Environ. Health. Perspect., 112(2): 186-200.

Becheri, A.; Durr, M.; Lo Nostro, P.; Baglioni, P.; (2008). Synthesis and characterization of zinc oxide nanoparticles: application to textiles as UV-absorbers. J. Nanopart. Res, 10(4): 679–689.

Casida, J.E.; & Quistad, G.B.; (2004). Organophosphate toxicology: safety aspects of nonacetylcholinesterase secondary targets. Environ. Chem. Toxicol. Lab., 17(8): 983–998.

Decker, S.P.; Klabunde, J.S.; Khaleel, A.; Klabunde, K.J.; (2002). Catalyzed destructive adsorption of environmental toxins with nanocrystalline metal oxides. fluoro-, chloro-, bromocarbons, sulfur, and organophosophorus compounds. Environ. Sci. Technol., 36(4): 762-768.

Eskandari, A.; Anbia, M.; Jahangiri, M.; Mohammadi Nejati, F.; (2017). Investigation of the use of various silica sources on NaX zeolite properties. J. Chem. Petrol. Eng., 50(1): 1-7.

Ghosh, M.; Rao, C.N.R.; (2004). Solvothermal synthesis of CdO and CuO nanocrystals. Chem. Phys. Lett., 393(4-6): 493-497.

Ghosh, P.K.; Maity, R.; Chattopadhyay, K.K.; (2004). Electrical and optical properties of highly conducting CdO:F thin film deposited by sol–gel dip coating technique. Sol. Energy Mater Sol. Cells., 81(2): 279-289.

Gordon, W.O.; Tissue, B.M.; Morris, J.R.; (2007). Adsorption and decomposition of dimethyl methylphosphonate on Y_2O_3 nanoparticles. J. Phys. Chem. C., 111(8):3233-3240.

Ismail, A.A.; El-Midany, A.; Abdel-Aal, E.A.; El-Shall, H.; (2005). Application of statistical design to optimize the preparation of ZnO nanoparticles via hydrothermal technique. Mater. Lett., 59(14-15): 1924-1928.

Kanaly, R.A.; kim, I.S.; Hur, H.G.; (2005). Biotransformation of 3-methyl-4-nitrophenol, a main product of the insecticide fenitrothion, by aspergillus niger, J. Agric. Food Chem., 53(16): 6426–6431.

Kaviyarasu, K.; Manikandan, E.; Paulraj, P.; Mohamed S.B.; Kennedy J.; (2014). One dimensional

well-aligned CdO nanocrystal by solvothermal method. J. Alloys. Compd., 593(1): 67-70.

Krishnakumar, T.; Jayaprakash, R.; Prakash, T.; Sathyaraj, D.; Donato, N.; Licoccia, S.; Latino, M.; Stassi, A.; Neri, G.; (2011). CdO-based nanostructures as novel CO2 gas sensors. Nanotechnol., 22(32): 325501.

Kosanovic, C.; Havancsák, K.; Subotic, B.; Svetlicic, V.; Radic, T.M.; Cziráki, A.; Huhn, G.; Buljan, I.; Smrecki, V.; (2011). Study of the mechanism of formation of nano-crystalline zeolite X in heterogeneous system. Microporous Mesoporous Mater., 142(1): 139-146.

Jadduaa, M.H.; Habubi, N.F.; Ckal, A.Z.; (2016). Preparation and Study of CdO-CdO2 Nano particles for Solar Cells Applications. Int. Lett. Chem. Phys. Ast., 69(1): 34-41.

Li, Y.X.; Koper, O.; Atteya, M.; Klabunde, K.; (1992). Adsorption and decomposition of organophosphorus compounds on nanoscale metal oxide particles. In situ GC-MS studies of pulsed microreactions over magnesium oxide. Chem. Mater., 4(2): 323-330.

Meaklim, J.; Yang, J.; Drummer, O.H.; Killalea, S.; Staikos, V.; Horomidis, S.; Rutherford, D.; Ioannides-Demos, L.L.; Lim, S.; McLean, A.J.; McNeil, J.J.; (2003). Fenitrothion: toxicokinetics and toxicologic evaluation in human volunteers. Environ. Health. Perspect., 111(3): 305-308.

Ning, G.h.; Zhao, X.P.; Li, J.; (2004). Structure and optical properties of MgxZn1−xO nanoparticles prepared by sol–gel method. Opt. Mater., 27(1): 1-5.

Panayotov, D.A.; Morris, J.R.; (2009). Thermal decomposition of a chemical warfare agent simulant (DMMP) on TiO_2: adsorbate reactions with lattice oxygen as studied by infrared spectroscopy. J. Phys. Chem. C., 113(35): 15684-15691.

Quinn, D.M.; (1987). Acetylcholinesterase: enzyme structure, reaction dynamics, and virtual transition states. Chem. Rev., 87(5): 955–979.

Raushel, F.M.; (2002). Bacterial detoxification of organophosphate nerve agents. Curr. Opin. Microbiol., 5(3): 288–295.

Saiedi, M;, Sayyadnejad, M.A.; Rashidi, A.M.; (2011). Synthesis of ZnO nanoparticles by spray pyrolysis method. Iran. J. Chem. Chem. Eng., 30(1): 1-6.

Silva, J.A.C.; Schumann, K.; Rodrigues, A.E.; (2012). Sorption and kinetics of CO2 and CH4 in binderless beads of 13X zeolite. Microporous Mesoporous Mater., 158(1): 219-228.

Sebastian, J.; Jinka, K.M.; Jasra, R.V.; (2006). Effect of alkali and alkaline earth metal ions on the catalytic epoxidation of styrene with molecular oxygen using cobalt(II)-exchanged zeolite X. J. Catal., 244(2): 208–218.

Somiya, S.; Roy, R.; (2000). Hydrothermal synthesis of fine oxide powders. Bull. Mater. Sci., 23(6): 453-460.

Su, L.M.; Grote, N.; Schmitt, F.; (1984). Diffused planar InP bipolar transistor with a cadmium oxide film emitter. Electron. Lett., 20(18): 716-717.

Tadjarodi, A.; Imani, M.; (2011). Synthesis and characterization of CdO nanocrystalline structure by mechanochemical method. Mater. Lett., 65(6): 1025-1027.

Tadjarodi, A.; Imani, M.; Kerdari, H.; (2013). Application of a facile solid-state process to synthesize the CdO spherical nanoparticles. Int. Nano Lett., 3(43): 1-6.

Tamura, H.; Maness, S.C.; Reischmann, K.; Dorman, D.C.; Gray, L.E.; Gaido, K.W.; (2001). Androgen receptor antagonism by the organophosphate insecticide fenitrothion. Toxicol. Sci., 60(1): 56-62.

Tripathi, R.; Dutta, A.; Das, S.; Kumar, A.; Sinha, T.P.; (2016). Dielectric relaxation of CdO nanoparticles. Appl Nanosci., 6(2): 175–181.

Wu, X.; Coutts, T.J.; Mulligan, W.P.; (1997). Properties of transparent conducting oxides formed from CdO and ZnO alloyed with SnO2 and In2O3. J. Vac. Sci. Technol., 15(3): 1057.

Yang, Y.; Chen, H.; Zhao, B.; Bao, X.; (2004). Size control of ZnO nanoparticles via thermal decomposition of zinc acetate coated on organic additives. J. Cryst. Growth., 263(1-4): 447-453.

Yang, Z.X.; Zhong, W.; Yin Y.X.; Du, X.; Deng, Y.; Au, C.; Du, Y.W.; (2010). Controllable synthesis of single-crystalline CdO and Cd(OH)2 nanowires by a simple hydrothermal Approach. Nanoscale Res. Lett., 5(1): 961–965.

Yekta, S.; Sadeghi, M.; Babanezhad, E.; Shahabfar, N.; (2014). Preparation of sodium dodecyl sulfate

modified pyrrolidine-1-dithiocarboxylic acid ammonium coated magnetite nanoparticles for magnetic solid phase extraction of Pb(II) from water samples. Int. J. Bio-inorg. Hybrid Nanomater., 3(3): 143-156.

Yi, H.; Deng, H.; Tang, X.; Yu, Q.; Zhou, X.; Liu, H.; (2012). Adsorption equilibrium and kinetics for SO_2, NO, CO_2 on zeolites FAU and LTA. J. Hazard. Mater., 203-204(1): 111-117.

Yufanyi, D.M.; Tendo, J.F.; Ondoh, A.M.; Mbadcam, J.K.; (2014). CdO nanoparticles by thermal decomposition of a cadmium- hexamethylenetetramine complex. J. Mater. Sci. Res., 3(3): 1-11.

AUTHOR (S) BIOSKETCHES

Sina Yekta, M.Sc., Instructor, Department of Chemistry, Payame Noor University (PNU), Tehran, Iran

Meysam Sadeghi, Ph.D., Department of Chemistry, Lorestan University, Khorramabad, Iran, *Email: meysamsadeghi1177@gmail.com*